

Overview of TCV Results

H. Weisen, S. Alberti, C. Angioni, K. Appert, J. Bakos¹, R. Behn, P. Blanchard, P. Bosshard, R. Chavan, S. Coda, I. Condrea, A. Degeling, B. P. Duval, D. Fasel, J.-Y. Favez, A. Favre, I. Furno, P. Gomez, T.P. Goodman, M. A. Henderson, F. Hofmann, R.R. Kayruthdinov², P. Lavanchy, J. B. Lister, X. Llobet, A. Loarte³, V.E. Lukash⁴, P. Gorgerat, J.-P. Hogge, P.-F. Isoz, B. Joye, J.-C. Magnin, A. Manini, B. Marlétaz, P. Marmillod, Y. Martin, An. Martynov, J.-M. Mayor, E. Minardi⁵, J. Mlynar, J.-M. Moret, P. Nikkola, P. J. Paris, A. Perez, Y. Peysson⁶, Z.A. Pietrzyk, V. Piffi⁷, R.A. Pitts, A. Pochelon, H. Reimerdes, J.H. Rommers, O. Sauter, E. Scavino, A. Sushkov², G. Tonetti, M.Q. Tran and A. Zabolotsky

Centre de Recherches en Physique des Plasmas
Association EURATOM-Confédération Suisse
École Polytechnique Fédérale de Lausanne
CH-1015 Lausanne, Switzerland

¹ KFKI, Budapest, HU; ²RRC, Moscow, RUS; ³EFDA-CSU, Garching, D;
⁴TRINITI, Troisk, RUS; ⁵Istituto di Fisica del Plasma “P.Caldirola”, Milano, I;
⁶CEA, Cadarache, F; ⁷IPP, Prague, CZ

E-mail address of main author: Henri.Weisen@epfl.ch

Abstract. The TCV tokamak ($R=0.88\text{m}$, $a<0.25\text{m}$, $B_T<1.54\text{T}$) is equipped with six 0.5MW gyrotron sources operating at 82.7 GHz for second harmonic X-mode ECH. By distributing the ECCD current sources over the discharge cross section, fully driven stationary plasmas with $I_p=210\text{kA}$, $n_{e0}=2\cdot 10^{19}\text{m}^{-3}$, $T_{e0}\approx 4\text{keV}$, were obtained for the full discharge duration of 2s. Highly peaked electron temperature profiles with T_{e0} up to 12keV were obtained in central counter current drive scenarios with off-axis ECH. Absorption measurements using a 118 GHz gyrotron have demonstrated the importance of suprathreshold electrons for third harmonic absorption. A coupled heat-particle transport phenomenon known as “density pumpout”, which leads to the expulsion of particles from the plasma core, has been linked to the presence of $m=1$ modes, suggesting that it is due to the existence of locally trapped particles associated with the loss of axisymmetry. Highly elongated discharges have been developed with Ohmic heating ($\kappa<2.8$) and off-axis ECH. The latter exhibit considerably improved vertical stability due to current profile broadening. A “gateway” for Elmy H-modes has been discovered, which allows stationary Ohmic ELMy H-mode operation in over wide range of elongation, triangularity and density. Divertor detachment experiments suggest the existence of recombination pathways other than three-body or radiative processes.

1. Recent Advances

The TCV (Tokamak à Configuration Variable, $R=0.88\text{m}$, $a<0.25\text{m}$, $B_T<1.54\text{T}$) with a vessel elongation of 3, was designed to be a highly versatile facility destined for the investigation of the effects of plasma shaping on confinement and stability [1]. Following the installation of a flexible ECH heating and current drive system, now totalling 2.8MW of power available to the plasma at the second cyclotron harmonic (82.7GHz), TCV has delivered significant achievements to the fusion community. One of the most important of these is probably the first demonstration of steady-state fully non-inductive ECCD operation for 2s at plasma currents of up to 210 kA [2,3]. These experiments also established the necessity of tailoring the driven current profile by suitably distributing the six available sources over the plasma cross section in order to avoid disruptive MHD instabilities and have provided a first validation of theoretical predictions for ECCD efficiencies in steady-state conditions.

ECCD and ECH also have proven to be powerful tools for current profile modification for the purpose of establishing and controlling improved core confinement (ICC) modes and for improving vertical stability at high elongation. Reversed or weak central shear discharges at moderate elongation ($\kappa \sim 1.7$), produced by central counter-current drive (CNTR-ECCD) in combination with off-axis ECH for improving MHD stability, have led to stable electron confinement enhancements $H_{RLW} = 3.5$ over Rebut-Lallia-Watkins scaling, limited in duration by the length of the ECH pulse. With Ohmic heating alone, the most elongated plasmas can only be vertically stabilized at high plasma current and the highest elongation achieved so far is 2.8 with an edge safety factor $q_{95} = 2.5$. The addition of a moderate level of off-axis ECH power (1MW) has recently allowed the minimum stable plasma current for $\kappa_a = 2.4$ to be reduced three-fold to 300kA, corresponding to $q_{95} = 8.2$. These experiments open up a wide and promising operational domain for future investigation of improved confinement modes at high elongation.

Investigations of the scaling of sawtooth inversion radii and profile shapes have revealed that these depend solely on the parameter $\langle j \rangle / q_0 j_0$ (defined in section 6) in Ohmic plasmas and both on this parameter and the deposition profile with ECH/ECCD. The results show that, due to the significant effect of the central elongation, current profile width and inversion radii do not become excessive at high elongation. A study of sawtooth behaviour as a function of elongation revealed a marked decrease of sawtooth periods and crash amplitudes for $\kappa_a > 2$, both with ECH and in purely Ohmic plasmas, attributed to a reduced internal kink stability margin.

The first of three gyrotrons, destined for operation at the third harmonic X-mode (118GHz), has been brought into service for physics investigations of the role of target plasma conditions on wave absorption. These experiments have demonstrated that absorption of X3 power is vastly enhanced when a suprathermal electron population produced by X2-ECCD is present in the plasma. Total absorption (within 10% error bars) was achieved for the 470kW of injected X3 power with as little as 350kW of X2-ECCD for target plasma conditioning, as compared to 25% absorption with the same power of X2-ECH.

Although Ohmic H-modes are easy to obtain in TCV, even with the ion ∇B drift direction away from the X-point, transitions to steady-state ELMy H-modes are only obtained in a narrow region of the operational domain. Remarkably, after such a transition this attractive confinement mode is very resilient to subsequent changes of elongation and density.

Detachment in open divertor geometries and pure deuterium is found to be easier than expected from simulations, suggesting important contributions from recombination pathways other than three-body and radiative processes.

TCV has also been used as a test-bench for the non-linear evolution code DINA [2] with the purpose of validating it for ITER poloidal field coil feedback controller design.

2. Fully Non-Inductive Operation with ECCD

The six ECH launchers in TCV allow independent steering of the heating sources in both the poloidal and toroidal directions; this high flexibility matches that of the TCV control system, permitting the entire vast range of shapes that can be created to be heated in an accurately localized manner. The six sources can be employed to tailor the current profile in a stationary manner, as will be required in a prospective reactor for MHD stabilization and optimization of performance. Crucial to the stationarity requirement is the ECH pulse length capability which substantially exceeds the current redistribution time from Ohmic to non-inductively driven profiles (typically < 0.5 s).

Studies have been carried out over the past year in TCV at increasing power levels to demonstrate stable, steady-state current profile control and to validate ECCD physics. After the first demonstration of fully non-inductive operation in steady state with ECCD in a tokamak was performed in TCV [3], work has progressed to a present record non-inductively driven current of 210 kA [4], shown in Fig. 1. The current is sustained non-inductively for 2 s, while plasma conditions relax over a time scale of less than 0.5 s. The current in the Ohmic transformer primary is kept constant by feedback throughout the ECCD pulse; thus, in the stationary phase during which the currents in all the shaping coils are also constant, no flux supplied to the plasma. The bootstrap current fraction is calculated to be 8% in this discharge. The conventional normalized ECCD efficiency of the discharge in Fig. 1 corresponds to 0.0073 [10^{20} A/W/m²]. Higher efficiencies, up to 0.016 in the same units, have been obtained by concentrating all sources in the centre, but such discharges become MHD unstable and disrupt. It was experimentally found that at each power level there is a minimum stable driven current profile width, below which such MHD instabilities develop and lead to disruption. As these instabilities are driven by current or pressure gradients, which increase with power for constant profile shape, the deposition width must be increased with increasing power. This results in an effective degradation of the maximum global ECCD efficiency with power. By way of illustration of this effect, Fig. 2 shows the power and current deposition profiles calculated by the linear ray tracing code TORAY [5] (with the Cohen package [6] for current drive estimation) for the case of Fig. 1 and for a case with similar plasma conditions but only three sources (1.35 MW) and a steady-state non-inductive current of 160 kA. Each case corresponds to the narrowest stable deposition profile identified over a series of discharges at each power level.

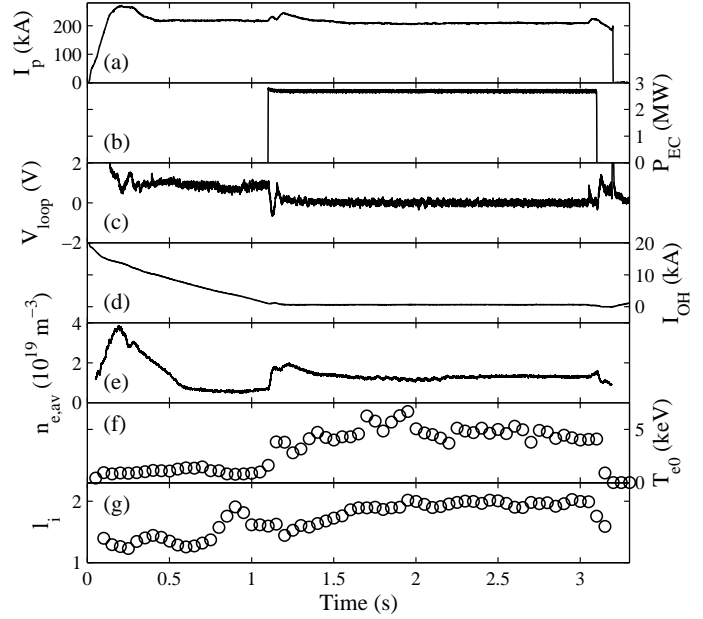


Fig. 1 Steady-state, fully non-inductive 210 kA discharge in a single-null diverted plasma with 2.8 MW of distributed ECCD: time histories of (a) plasma current, (b) EC power, (c) edge loop voltage, (d) current in the Ohmic transformer primary, (e) line-averaged density, (f) peak electron temperature, (g) internal inductance

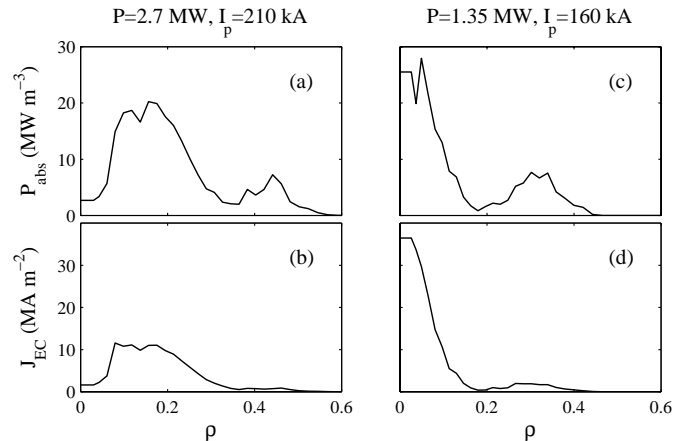


Fig. 2 Flux-surface-averaged (a)-(c) absorbed power and (b)-(d) driven current density as functions of a normalized radial coordinate proportional to the square root of the plasma volume, for two different discharges. All profiles are calculated by TORAY. Line-averaged density $1 \times 10^{19} \text{ m}^{-3}$ (a-b) and $1.2 \times 10^{19} \text{ m}^{-3}$ (c-d), central electron temperature 3.1 keV (a-b) and 3.7 keV (c-d).

The fundamental principles of ECCD have been known for twenty years [7] but a thorough experimental validation is still missing. One of the principal aims of the ongoing experiments on TCV is to provide that validation, particularly through measurements of the ECCD efficiency $\eta = I_{EC}/P$. I_{EC} is the driven current and P the EC power, has the theoretical dependence $\eta = T_e \eta_T' / [R n_e (Z_{eff} + 5)]$, where T_e is the electron temperature, R is the major radius, n_e is the density, Z_{eff} is the effective ion charge and η_T' is a function of the trapped particle fraction and of the parallel wave number [7]. The dependence on the trapped particle fraction in particular is predicted to be strong and to result in a rapid reduction of η_T' with increasing minor radius. The average efficiencies measured on TCV in a series of fully non-inductive discharges with varying deposition profile widths have shown up a dependence on the minor radius of the magnitude predicted by theory, giving a clear indication of the existence of trapped particle effects [4]. Furthermore, the absolute value of η_T' agrees with predictions by the linear TORAY code to within 30%, over a range of profiles resulting in a variation in η_T' of a factor of 3.5. Nonlinear effects thus do not appear to be significant in the present conditions.

3. Quasi-Stationary Improved Core Confinement by Shear Optimization

An Improved Core Confinement (ICC) regime has been obtained by current profile tailoring with ECH and ECCD in quasi-steady state conditions [9]. The intense central counter current drive (CNTR-ECCD) produced in the ICC regime and related equilibrium modelling suggest the presence of a strong reverse shear profile in the plasma core. In most tokamak experiments reversed shear profiles are obtained only transiently by heating during the ramp-up phase of the plasma current. Taking advantage of the very localized power deposition, which is typical of ECH, and making use of the flexibility of the beam launching system on TCV, an optimized current density profile could be established and maintained for the duration of the heating pulse, corresponding to 200 energy confinement times and several current redistribution times. For this purpose a combination of 4-5 X2 heating beams was used to deliver a total power in the range 1.8-2.3 MW to the plasma. The optimized scenario begins with off-axis heating just outside the $q=1$ surface using two or three X2 beams followed 300 ms later by central power deposition with a strong counter current drive (CNTR-ECCD) component using two beams. The discharge evolution is shown in Fig. 3 for two examples with central CNTR-ECCD and for central ECH. Typical plasma parameters were $\delta_{95} \approx 0.2$, $\kappa_{95} \approx 1.6$, $q_{95} \approx 6$, $I_p \approx 200$ kA and $\langle n_e \rangle \approx 1.5 \times 10^{19} \text{ m}^{-3}$. Central CNTR-ECCD leads to significantly higher peak electron temperatures (8-12 keV) than central ECH (~ 4 keV) and better global plasma performance. The delay between the beginning of the off-axis ECH and the on-axis CNTR-ECCD, which is of the order of the current redistribution time, is necessary to establish a suitably broad and MHD stable target current profile for the central CNTR-ECCD pulse. If the delay is reduced to zero, or if the off-axis ECH is altogether omitted [9], high temperatures (~ 10 keV) can also be obtained, although these discharges are often violently sawtoothing and disruptive.

The achieved electron energy confinement times exceed the one predicted by the Rebut-Lallia-Watkins (RLW) scaling law by a factor of 3.5, as seen in Fig. 3b. Unlike discharges with central CNTR-ECCD only, these ICC plasmas are MHD quiescent, like #18639 in Fig. 3 and #18518 in Fig. 4, or else only exhibit benign levels of sawtooth activity, like #18635 in Fig. 3, with crash amplitudes of ~ 3 keV and periods of ~ 20 ms, which far exceed the global energy confinement time of ~ 5 ms. In the absence of direct measurements of the current density profile, the evolution of the q -profile and its relation to the reduction in transport coefficients is inferred from time dependent simulations [11] using the PRETOR code [12] and the RLW local transport model. The RLW transport parameters depend strongly on the magnitude of the

magnetic shear, but are assumed not to depend on its sign. An example is presented in Fig. 4a, with simulated temperature profiles for the Ohmic, off-axis ECH and high performance ICC phases, together with the experimental data from Thomson scattering, showing good agreement. Within the framework of the local RLW heat diffusivity model, used in these calculations, the negative shear zone near the center is essential for the confinement enhancement [11]. The corresponding q-profiles in Fig. 4b show reversed shear during the central counter ECCD phase. The central CNTR-ECCD current is calculated to be 125kA. The range of plausible q-profiles has been computed by PRETOR used as a fixed-boundary equilibrium solver (without transport model) constrained by the experimental density and temperature profiles, the effective ion charge, the edge loop voltage, and reflects the high sensitivity of the calculation to the location of the CNTR-ECCD source taken from TORAY calculations. This sensitivity to the ECCD source location has motivated an experimental scan of the position of the CNTR-ECCD component which has shown that an outward displacement of only 10% of the minor radius caused a 40% reduction in the central plasma temperature, which is also borne out by the PRETOR simulations [13].

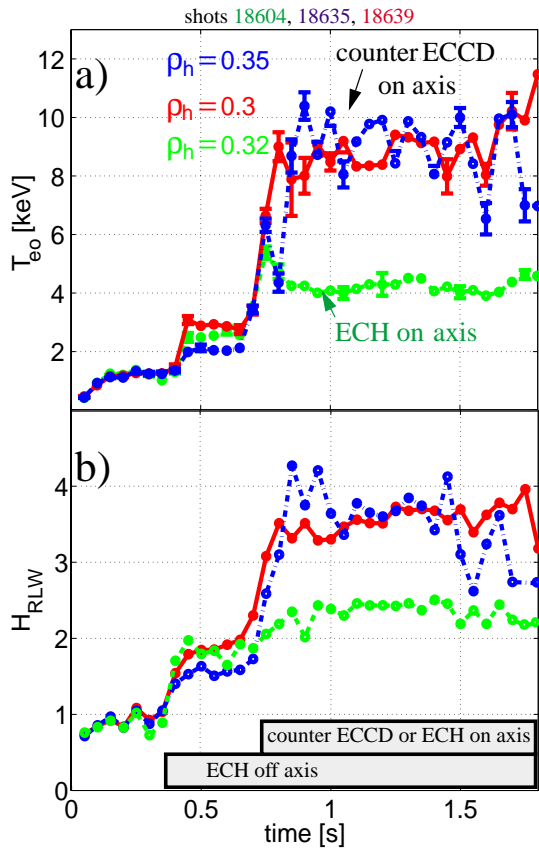


Fig. 3 a) Evolution of central electron temperature from Thomson scattering and b) enhancement factor over RLW energy confinement time for different ECH/CNTR-ECCD scenarios combining off-axis ECH (0.9MW) at different locations ρ_h with delayed central ECH or CNTR-ECCD. green: with 0.9MW central ECH blue and red: with 0.9 MW central CNTR-ECCD

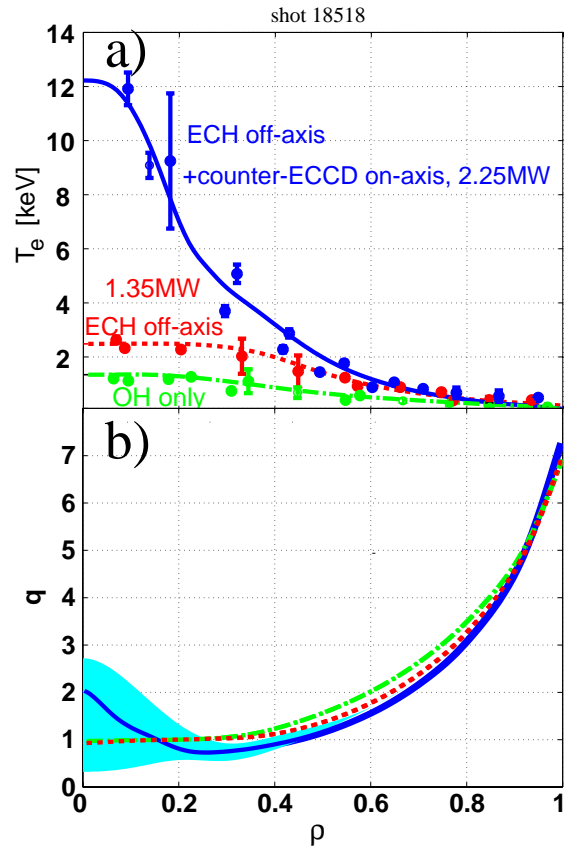


Fig. 4 a) Electron temperature profiles as simulated using RLW transport model for 3 phases of an ICC shot, together with measurements. Fig. 5 green: OH phase, red: 1.35 MW off-axis ECH, blue: combination off-axis ECH and 0.9MW central CNTR-ECCD. b) Corresponding calculated safety factor profiles with uncertainties (shaded) related to location of central CNTR-ECCD sources.

4. Full Absorption of ECH Power at the Third EC Harmonic in X-Mode

Plasmas in the TCV Tokamak have, for the first time, been heated using the first of three 0.5MW gyrotrons to be deployed at a frequency of 118 GHz [14], corresponding to the third EC harmonic. One of the motivations for X3 ECH in TCV is the possibility of heating at densities which are inaccessible with the X2 ECH system. The experiments reported here were aimed at establishing the importance of the plasma conditions, mainly electron temperature and suprathermal tail electron distributions, for the absorption of X3 ECH power [15]. For this purpose the plasmas were preheated with different power levels of X2 ECH and ECCD. The X3 wave was launched from the low field side via one of the upper lateral launching mirrors normally used for X2 heating [16].

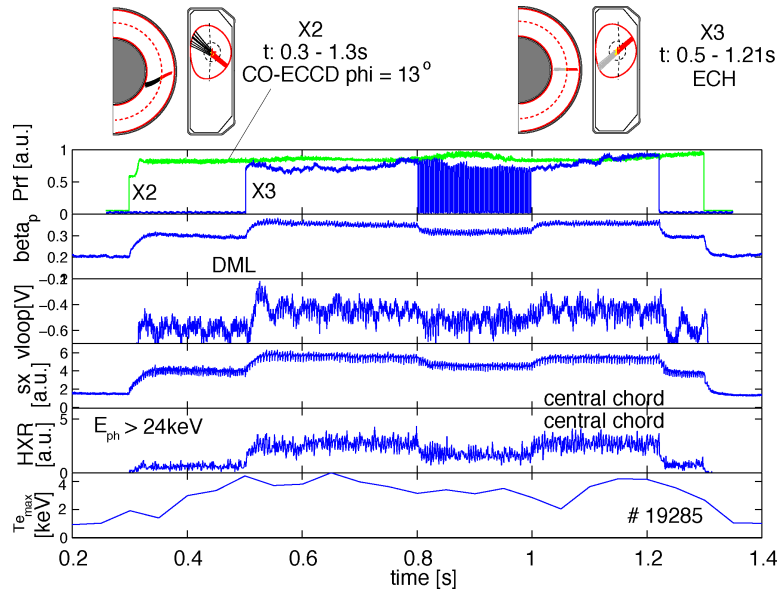


Fig. 6 Launching geometry and typical time traces for the X2 and X3 ECH. Top to bottom: RF power, poloidal beta, loop voltage, soft X-ray signal, hard X-ray signal, peak electron temperature. $P_{X2}=P_{X3}=0.47M$, $I_p=200kA$.

The total stored energy variation was measured during the modulated part of the X3 RF pulse using a diamagnetic loop. The modulation frequency of $f_m=237Hz$ was chosen such that $1/2\pi f < \tau_e \sim 5ms$, where τ_e is the electron energy confinement time. While the X3 power (0.47MW) and launching geometry, aimed at the plasma centre, were kept constant, different X2 conditions were investigated, including variations of the toroidal launch angle ϕ , the power deposition radius, the total X2 power and the plasma current. A toroidal injection angle scan of the X2 launch, with $P_{X2} \approx P_{X3} = 0.47MW$, has revealed a clear asymmetry. X3 absorption is highest on target plasmas with X2 injected with $\phi = +13^\circ$, corresponding to CO-ECCD. Fig. 7 shows the X3 absorbed power fraction, versus X2 preheat power for three X2 launching angles corresponding to CO-ECCD ($\phi = 13^\circ$), ECH ($\phi = 0^\circ$) and CNTR-ECCD ($\phi = -13^\circ$). For CO-ECCD target plasmas, nearly 100% absorption is obtained.

Calculations of the theoretical absorption with the TORAY ray tracing code [5], which makes the assumption of an isotropic, Maxwellian velocity distribution, are in fair agreement with the experimental results corresponding to ECH preheating. This observation is also in agreement with X3 absorption measurements by Pachtman et al. [17]. However, the measured X3 absorption exceeds that predicted by TORAY by a factor of up to 3 for the CNTR- and CO-ECCD cases. The only explanation of the discrepancy is that a large fraction of the X3 power is

The target plasmas used in these experiments have the parameters $R=0.88m$, $a=0.25m$, $\kappa=1.31$, $B_0 = 1.42T$, $n_e(0) = 2.5 \times 10^{19} m^{-3}$. The launching geometry and time traces of relevant parameters are shown in Fig. 6 for a typical discharge. The top trace shows the timing X2 ECCD and X3 ECH. In all experiments the X2 power was kept constant from 0.3s to 1.3s whereas the X3 power was applied from 0.5s to 1.2s and included a phase with 100% modulation at 237Hz (0.8s to 1s).

absorbed by energetic tail electrons created by X2 ECCD. The presence of these is confirmed by the measurement of photon spectra using an energy resolving hard X-ray camera and a high field side ECE radiometer. The ECE radiometer detects suprathermal radiation levels exceeding the thermal level by an order of magnitude, while effective X-ray photon temperatures of tens of keV are measured in the presence of ECCD and X3 ECH. The insert in Fig. 7 shows that hard X-ray ($>10\text{keV}$) emission is highest with X2 CO-ECCD and lowest with X2 ECH in all phases of the experiment.

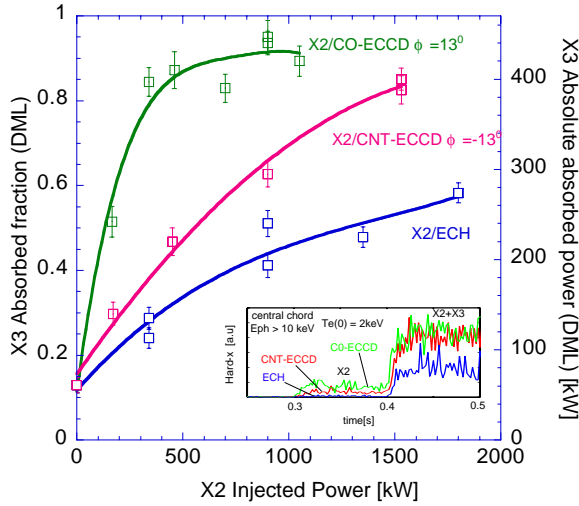


Fig. 7 Measured X3 absorption using the DML versus X2 preheat power for three different X2 launching configurations:

- CO-ECCD (green, $\phi=13^\circ$),
- CNTR-ECCD (red, $\phi=-13^\circ$),
- and ECH (blue, $\phi=0^\circ$).

3^{rd} harmonic ECH ($\phi=0^\circ$) is kept constant at 0.47MW with central deposition.

Insert shows hard X-ray ($>10\text{keV}$) signals for X2 Co- (green) and CNTR-ECCD (red) as well as X2 ECH (blue) cases. X3 ECH is applied from 0.4 s when the large rise in hard X-ray emission is observed.

The toroidal angle asymmetry suggests that the Ohmic electric field may also play an

important role in shaping the energetic tail electron velocity distribution. This hypothesis is confirmed by ECE, hard X-ray and absorption measurements in a loop voltage scan in the range $0.23\text{-}0.55\text{V}$, obtained by varying the plasma current from $130\text{-}230\text{ kA}$, with $\phi=13^\circ$. Absorption decreases significantly as the loop voltage is reduced.

5. Particle Transport with High Power ECH and ECCD

A coupled heat and particle transport phenomenon, leading to particle depletion from the plasma core is observed in a variety of plasma conditions with centrally deposited ECH and ECCD in TCV. This phenomenon, known as “density pumpout” causes inverted density sawteeth in the core of sawtoothing discharges and leads to stationary hollow profiles in the absence of sawteeth. The density pumpout has been linked to the presence of $(n,m)=(1,1)$ MHD modes and can be suppressed by stabilizing the mode by means of operation at high triangularity. The correlation of pumpout with loss of axisymmetry suggests that neoclassical transport processes involving locally trapped particles other than those arising from the toroidal field ripple and analogous to those in heliacs, may account for the phenomenon in tokamaks as well.

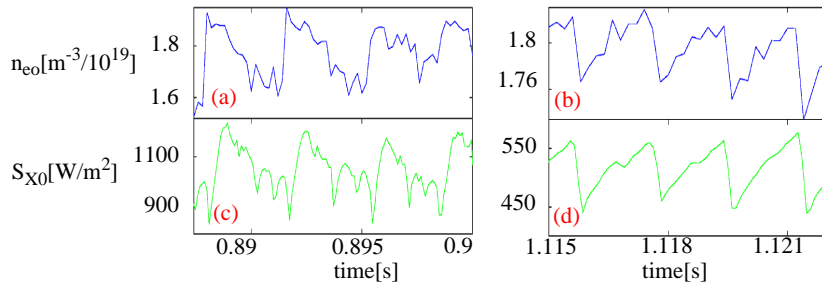


Fig. 8 Sawteeth on central Abel-inverted density (top) and raw X-ray signal (bottom) for Ohmic heating (left) and ECH (right) with $\delta_a=0.22$ and $P_{\text{ECH}}=1.45\text{MW}$.

Fig. 8 shows the difference in sawtooth behaviour at low and high heating power at low triangularity. For $P_{\text{ECH}}>0.5\text{ MW}$ density sawteeth are inverted. The situation is different at high triangularity ($\delta_a>0.3$) when both X-ray traces and central densities have “normal”, triangular sawteeth. The essential difference appears to be that at low triangularity a $(1,1)$ magnetic island

is present during the sawtooth ramp phase, whereas the plasma is MHD-quiescent during the ramp phase at high triangularity.

The convective heat flux associated with the “pumped-out” particles is a small fraction, estimated to be less than 10%, of the loss power from the core. In sawtoothed plasmas strongly hollow density profiles cannot develop because the sawtooth crashes regularly flatten density and temperature profiles. However with ECCD many situations arise when sawteeth are stabilized for long enough (typically 10 ms or more) for the hollowness to become significant enough for the Thomson scattering system, as shown in Fig. 9.

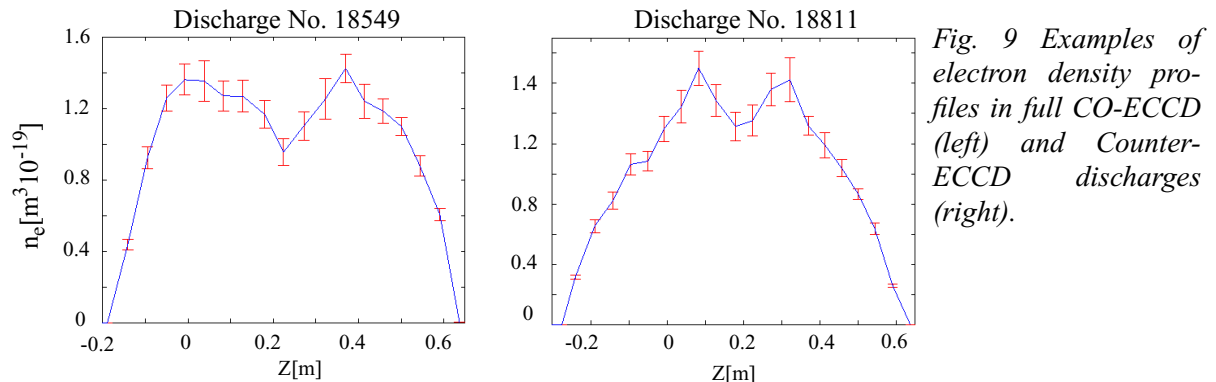


Fig. 9 Examples of electron density profiles in full CO-ECCD (left) and Counter-ECCD discharges (right).

One of the first explanations for “pumpout” in tokamaks by Hsu et al [18], based on the production of an excess of banana electrons and a poloidal charge asymmetry, is not consistent with our observations [19]. We propose that a loss of axisymmetry provides the crucial physics for this phenomenon by allowing the existence locally trapped particles, which are not confined in the core region. The presence of an $(n,m)=(1,1)$ island causes the core to be helically displaced. The vicinity of the displaced core acquires stellarator-like features. As a result trapped particle orbits exist even at the magnetic axis, just as in a heliac configuration. This region may act as a sink from where locally trapped particles are lost to beyond the non-axisymmetrical region (typically outside $q=1$). The coexistence of locally and toroidally trapped particles within the $q=1$ surface can also be expected to give rise to competing transport phenomena, including pumpout, since the neoclassical off-diagonal terms associated with these two classes of particles have opposite signs. Near the displaced axis the effect of locally trapped particles dominates, giving rise to an outward flux ($d_{12} \sim 1$ in the long mean-free path regime), while further away toroidally trapped particles ($d_{12} = -1/2$), or an anomalous mechanism, are most important, giving rise to an inward pinch [20].

6. Dependence of Inversion Radii and Peaking Factors on Plasma Shape

When considering highly elongated tokamak designs, a frequently expressed concern is that as a result of the high current carrying capacity of elongated plasmas, sawtooth in inversion radii and consequently crash amplitudes may become excessive. In Ohmic plasmas we observe that the normalised sawtooth inversion radius ρ_{inv} and the profile inverse peaking factors (normalised widths) $\langle p_e \rangle / p_{e0}$, $\langle T_e \rangle / T_{e0}$ and $\langle n_e \rangle / n_{e0}$ for electron pressure, temperature and density, depend on the current profile peaking via the parameter $\langle j \rangle / (q_0 j_0)$, where $\langle j \rangle$ is the cross-sectionally averaged current density, irrespective of plasma shape and electron density [22]. This parameter can be evaluated without knowledge of the still somewhat controversial value of the axial safety factor since $q_0 j_0 = B_0 (\kappa_0 + 1 / \kappa_0) / (\mu_0 R_0)$, where κ_0 is the axial elongation. The core elongation is generally in good agreement with the elongation of emissivity contours from X-ray tomography. In order to reduce the large scatter of the Thomson scattering measurements at random times in the sawtooth cycle we define “clipped” profile widths as

$\langle \bar{T}_e \rangle / T_{eI}$ where T_{eI} is the electron temperature at the sawtooth inversion radius and $\bar{T}_e = T_{eI}$ for $\rho < \rho_{inv}$ and $\bar{T}_e = T_e$ for $\rho \geq \rho_{inv}$. These widths are sensitive to the profile in the confinement zone ($q > 1$) and are shown in Fig. 10 for a wide variety of Ohmic and ECH L-mode plasmas [23]. The Ohmic data show a remarkably narrow distribution as a function of $\langle j \rangle / (q_0 j_0)$ and are in good agreement with an Ohmic relaxation model based on the assumption that the magnetic entropy is stationary in time [24]. The parameter $\langle j \rangle / (q_0 j_0)$ performs better than safety factor based scalings such as I/q_{95} , for which the dispersion is larger, and is related to the popular database variables q_{95} , κ_{95} and δ_{95} [23]. With ECH heating $\langle j \rangle / (q_0 j_0)$ remains the primary scaling parameter, but now the profiles are modified by the ECH heat deposition profiles, the widths of which are not matched in the experiments to $\langle j \rangle / (q_0 j_0)$.

TCV results show that frequently expressed fears of excessively large inversion radii and sawtooth amplitudes at high plasma elongation, susceptible to trigger NTM's, are ill founded. In TCV sawtooth amplitudes decrease with elongation both in Ohmic and in ECH heated discharges [21]. The normalized sawtooth inversion radius can be kept fixed while scaling up the plasma elongation κ_{95} , albeit at a modest penalty in plasma current (typically 10% for $\kappa_a = 2$), as compared to scaling at fixed q_{95} [23].

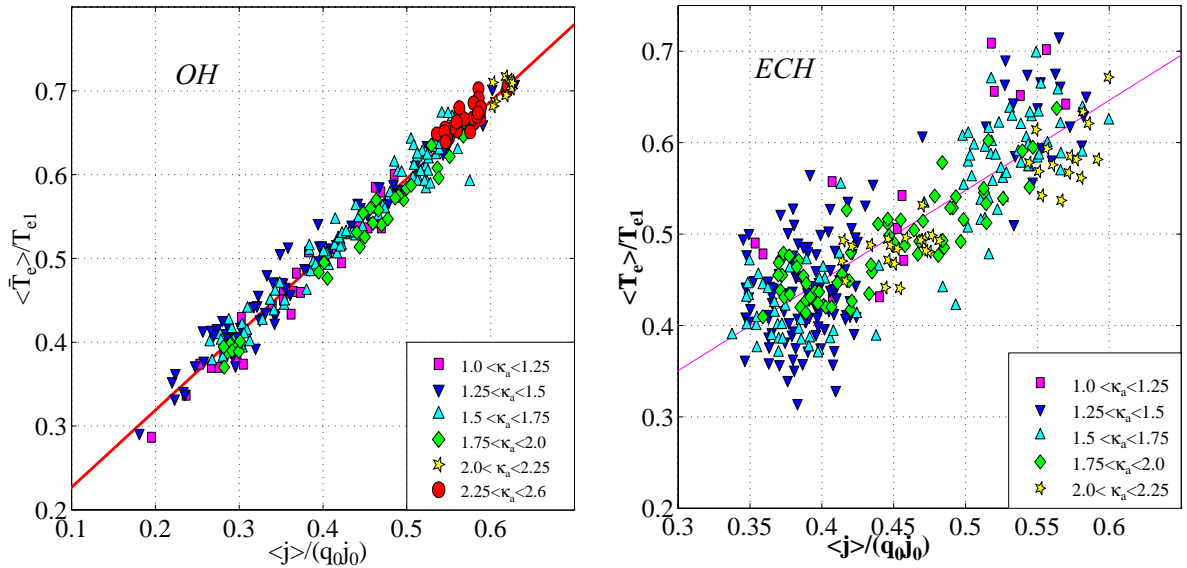


Fig. 10 Electron temperature inverse peaking factors in Ohmic (left) and ECH (right) plasmas.

7. Development of Highly Elongated Discharges

One of the main aims of the TCV tokamak is the creation and study of highly elongated plasmas. Part of the motivation for this comes from the fact that the maximum plasma current increases with elongation and according to Troyon scaling [25], the beta limit is proportional to the normalized current, $I_N = I / (aB_T)$. This favorable trend has been verified experimentally up to elongations of $\kappa = 2.3$ [26], but it is not known whether it continues to be valid at higher elongation. The creation of elongated plasmas with $\kappa > 2.5$ in a tokamak with conventional aspect ratio is an extremely difficult task [27]. In Ohmic plasmas, axisymmetrical stability imposes a lower limit to the normalized plasma current, which is necessary to produce a sufficiently broad current profile, and simultaneously, the non-axisymmetrical modes impose an upper limit to the current. The stable operating window between these two limits decreases as the elongation increases.

Axisymmetrical stability can be improved in several different ways. First, the passive stability can be improved by adapting the plasma shape as closely as possible to the shape of the vac-

uum vessel. Second, the vertical position control system can be optimized such that operation at very low stability margins becomes possible. Third, the current profile can be widened either by operating at the maximum possible plasma current, by using a fast ramp-up scenario or by applying off-axis ECH/ECCD. Non-axisymmetrical stability, on the other hand, can be improved by operating at low beta or at low current, since at high elongation, the current limit increases as beta decreases [28]. Clearly, the requirements for axisymmetrical and non-axisymmetrical stability are partially contradictory. As a result, beyond a certain elongation, the stable operating window shrinks to zero. Using the above methods in Ohmic plasmas, a maximum elongation $\kappa=2.8$ with $I_p/aB_T=3.6\text{MAm}^{-1}\text{T}^{-1}$ has been achieved in TCV (Fig. 11).

With Ohmic heating alone such extreme elongations have only been obtained at high values of normalized average current density, $\langle j \rangle^* = \mu_0 R_0 \langle j \rangle / B_T \sim 1.7$. With 1-2MW of ECH power deposited near or outside mid-radius, it is possible to create highly elongated plasmas with much lower values of $\langle j \rangle^*$ [29]. In the example of Fig. 12 plasma elongation was raised from $\kappa_a \approx 1.75$ to $\kappa_a = 2.4$ corresponding to $\langle j \rangle^* = 0.46$ and $\langle j \rangle / q_0 j_0 = 0.2$, just by applying the ECH power at fixed quadrupole field. The resulting broadening of the current profile leads to vastly improved vertical stability. The example presented has a temperature profile width $\langle T_e \rangle / T_{e0} \approx 0.4$, which is a factor ~ 1.5 times broader than obtained in Ohmic plasmas at the same value of $\langle j \rangle / q_0 j_0$. These experiments open up a wide operational domain for the investigation of confinement at high elongation.

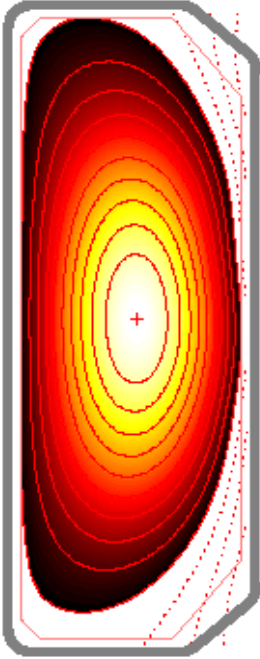


Fig. 11 (left)
Record elongation in TCV (#19373).
 $I_p=755\text{kA}$, $B_T=0.8\text{T}$, $\kappa_a=2.8$, $k_0=2.15$,
 $\delta_a=0.4$, $q_{95}=2.5$, $\langle j \rangle^*=1.74$

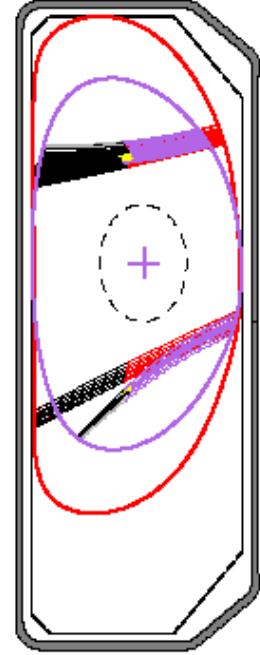


Fig. 12 (right)
ECH-assisted, highly elongated plasma (#19533).
Magenta: LCFS of initial configuration.
Red: LCFS of final elongated plasma with
 $I_p=300\text{kA}$, $B_T=1.43\text{T}$, $\kappa_a=2.4$, $q_{95}=8.3$,
 $\langle j \rangle^*=0.46$. ECH ray trajectories from
TORAY are also shown, parts beyond X2
resonance are in black.

8. Ohmic ELMy H-mode accessibility

Ohmic H-modes are easily obtained in TCV, even with ∇B away from the X-point. In most conditions these are ELM-free and terminate in a high density disruption. Transitions from L-mode to stationary ELMy H-modes for SN configurations with reversed ion ∇B are only observed (at the nominal field $B_T=1.43\text{T}$) in a narrow range of discharge parameters: $0.35\text{MA} \leq I_p \leq 0.43\text{MA}$, $4.5 \times 10^{19} \text{m}^{-3} \leq \langle n_e \rangle \leq 6 \times 10^{19} \text{m}^{-3}$, $1.6 \leq \kappa_a \leq 1.7$, $0.5 \leq \delta_a \leq 0.6$. Moreover the gap width between the inner wall and the plasma last closed flux surface must be between 1 and 3 cm. Outside this domain either L-modes or ELM-free H-modes are obtained. This would be very restrictive, were it not for the high robustness of the ELMy H-mode, once it is established. After the transition both the plasma elongation (together with the plasma current)

and the plasma density can be varied over a wide range as shown in Fig. 13 [30]. An ELM-insensitive magnetic position observer has been developed, which prevents an undesirable vertical controller response during the ELM events [31].

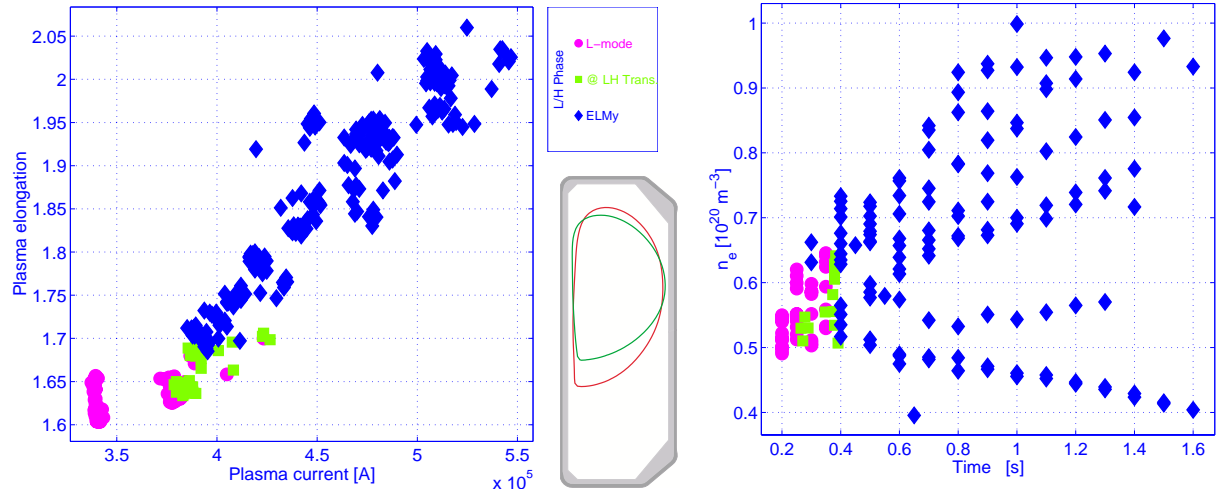


Fig. 13 Operational domain for ELMy SN H-modes. a) Accessible elongations and currents b) Accessible density (time evolutions). All discharges transited through a “gate” in the operational domain indicated by the green symbols. Central insert: LCFS at transition and at highest elongation.

9. Detachment in Variable Divertor Geometry

Although the requirement of shape flexibility precludes the use of fixed baffle or optimized divertor target structures, it does allow for the investigation of diverted equilibria not achievable in more conventional tokamaks. One such configuration, shown in Fig. 14, has been extensively used

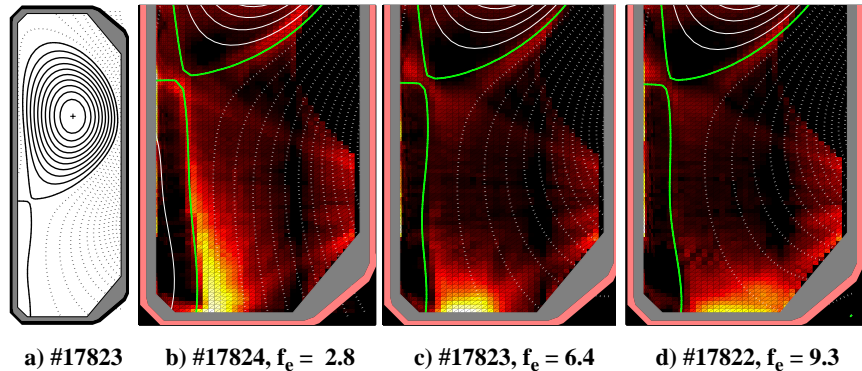


Fig. 14 Distributions of D_{α} emissivity for varying outer target flux expansion at the same degree of detachment.

for studies of divertor detachment in Ohmic conditions and unfavorable ∇B drift direction with deuterium fueling only [32]. The equilibrium is simultaneously characterized by a very short inboard poloidal depth from X-point to strike point on a vertical target and an extremely long poloidal depth to a horizontal target on the outboard side. Density ramp discharges, invariably terminated by an X-point MARFE, leave the inboard target plasma attached even at the highest densities, whilst clear partial detachment is observed at the outboard target. Extensive modelling of this configuration using the B2-EIRENE coupled package shows in fact that the outboard divertor achieves high recycling at very low densities, with the rollover to detachment occurring near the outer strike point very soon after the density ramp begins. The differences in detachment threshold at the two targets can be ascribed to a large extent to divertor magnetic geometry.

Whilst there is little latitude for changing the inboard geometry, a series of experiments has recently concentrated on studying the effect of outer target flux expansion, f_e , on the detachment behaviour. Fig. 14 (b,c,d) show inverted tangential CCD camera images of D_{α} emissivity from the divertor volume for the same absolute degree of detachment [33] as f_e

increases. The distributions clearly show the effect of plasma plugging by the expanded flux surfaces and can be qualitatively reproduced by code simulations. Interestingly, however, the latter find the maximum in the emissivity to be located at the strike point, in evident disagreement with experimental observation [34]. Moreover, the code cannot quantitatively reproduce the absolute level of detachment without artificially increasing fivefold the charged particle sink due to three-body and radiative recombination. This is a strong indication that other processes, perhaps involving molecularly assisted recombination pathways, dominate in the relatively low density plasma characterizing the TCV outer divertor. Such pathways are currently under further study.

Acknowledgement: This work was partly supported by the Swiss National Science Foundation.

References:

- [1] Hofmann F. et al., *Plasma Phys. Control. Fusion* **36** (1994) B277
- [2] Karyutdinov R.R and Lukash V.E., *J. Comp. Physics* **109** (1993) 193
- [3] Sauter O. et al, *Phys. Rev. Letters* **84** (2000) 3322
- [4] Coda S. et al, to be published in *Plasma Phys. Control. Fusion* (2000)
- [5] Kritz A.H. et al, *Proc. 3rd Varenna-Grenoble Int. Symposium on Heating in Toroidal Plasmas, Grenoble, 1982 (CEC, Brussels), vol. II, p. 707*
- [6] Cohen R. H., *Phys. Fluids* **30** (1987) 2442
- [7] Fisch N.J. and Boozer A.H., *Phys. Rev. Letters* **45** (1980) 720
- [8] Alikeev V.V. and Parail V.V., *Plasma Phys. Control. Fusion* **33** (1991) 1639
- [9] Pietrzyk Z.A. et al., *27th EPS Conf. Contr. Fusion and Plasma Phys., Budapest, 2000, P4.099*
- [10] Pietrzyk Z.A. et al., *Phys. Plasmas* **7** (2000) 2909
- [11] Angioni C. et al., to be publ. in *Theory of Fusion Plasmas*, Ed. Compositori, Bologna 2001
- [12] Boucher D. and Rebut P.H., in *Proc. IAEA Tech. Conf. on Advances in Simulation and Modelling in Thermonuclear Plasmas*, Montréal, 1992
- [13] Goodmann T.P. et al., this conference, paper EXP4/09
- [14] Alberti S. et al, to be published in *Fusion Engineering Design*
- [15] Alberti S. et al, this conference, PD/2
- [16] Goodmann T.P. et al., In *Proc. 19th Symp. Fusion Technology* (Lisbon, 1996) Vol 1, Ed. C. Varandas and F. Serra (Amsterdam: Elsevier), p 565.
- [17] Pachtman A., Wolfe S.M., Hutchinson I.H., *Nuclear Fusion*, Vol.27, No.8, (1987)
- [18] Hsu J.Y. et al., *Phys. Rev. Lett.* **53** (1984) 564
- [19] Weisen H., Furno I., Goodman T. and TCV Team, this conference, PDP/6
- [20] Kovrizhnykh L.M., *Nucl. Fusion* **24** (1984) 851
- [21] Reimerdes H. et al, *Plasma Phys. Contr. Fusion* **42** (2000) 629
- [22] Weisen H. et al, *Plasma Phys. Contr. Fusion* **40** (1998) 1803
- [23] Weisen H., Furno I. and TCV Team, submitted to *Nucl. Fusion*, CRPP report LRP 685/00
- [24] Minardi E. and Weisen H., accepted for *Nuclear Fusion*, CRPP report LRP 669/00
- [25] Troyon F. et al., *Plasma Phys. Controlled Fusion* **26**, 209 (1984)
- [26] Lazarus E.A. et al., *Phys. Fluids* **B4**, 3644 (1992)
- [27] Hofmann F. et al., *Nucl. Fusion* **28**, 399 (1998)
- [28] Hofmann F. et al., *Phys. Rev. Lett.* **81**, 2918 (1998)
- [29] Pochelon A. et al., this conference, paper EXP3/10
- [30] Martin Y. et al, this conference, EXP5/30
- [31] Hofmann F. et al, *27th EPS Conf. Contr. Fusion and Plasma Phys., Budapest, 2000, P1.029*
- [32] Pitts R.A. et al., to be published in *Journ. of Nucl. Mater.* (2000)
- [33] Loarte A. et al., *Nucl. Fusion* **38** (1998) 331
- [34] Pitts R.A. et al., this conference, paper EXP4/23